J. Fluid Mech. (1985), *vol.* 151, *pp.* 141–165
Printed in Great Britain

Wave motions on vortex cores

By T. MAXWORTHY†, E. J. HOPFINGER
Institut de Mécanique (Laboratoire Associé au CNRS), Université de Grenoble, B.P. n° 68, 38402 St Martin d'Hères Cedex, France

AND L. G. REDEKOPP
Department of Aerospace Engineering, University of Southern California, Los Angeles, CA 90089-1454, U.S.A.

(Received 30 June 1983 and in revised form 12 May 1984)

The observation of large-amplitude 'kink' waves on the vortex cores produced by an oscillating grid in a rotating fluid (Hopfinger, Browand & Gagne 1982) has motivated the study of such waves under more controlled circumstances. We have experimentally observed the properties of helical waves, rotating, plane standing waves and evolving, isolated kink-waves. Their characteristics have been related to theories based on the localized induction equation of Arms & Hama (1965), the 'cut-off' theory of Crow (1970) as extended by Moore & Saffman (1972), and an extension of Pocklington's (1895) dispersion relationship for 'hollow-core' vortices. It is shown that the latter dispersion relation and the Moore & Saffman theory are good approximations to our experimental results. Using these, we present new results on solitary kink-wave properties of concentrated vortex flows, and in particular show that envelope solitons are possible only for a restricted range of carrier wavenumbers. A second class of waves was also observed: the axisymmetric solitary waves of Benjamin (1967). These were found to become unstable to spiral disturbances when their amplitude exceeded a certain magnitude, as has been found in the study of the related vortex-breakdown phenomenon. All of these observations are used to interpret the experiments presented by HBG and to discuss qualitatively the dynamics of rotating turbulence. In the Appendix we propose a possible mechanism by which concentrated vortices can be formed in a rotating turbulent fluid.

1. Introduction

In a recently published paper Hopfinger, Browand & Gagne (1982, hereinafter referred to as HBG) generated a turbulent flow field in a cylindrical tank, rotating about a vertical axis with angular velocity Ω, by oscillating a grid of square bars at fixed frequency and excursion. Over a wide parameter range more-or-less equally spaced intense vortices, approximately aligned with the rotation axis, were formed and a variety of wave motions were then observed upon them. HBG concentrated almost exclusively on kinked solitary waves, and speculated on their importance in the overall dynamics of the system and in particular that they could be responsible for vortex intensification and vortex disruption. These conjectures and a broad interest in vortex motion and vortex breakdown phenomena motivated us to study travelling waves, in particular torsional waves, on isolated vortex cores.

The study of wave motions on vortex cores is a venerable one and, for many years,

† Permanent address: Departments of Mechanical and Aerospace Engineering, University of Southern California, Los Angeles, CA 90039-1453, U.S.A.

relatively simple solutions for the helicoidal wave (Pocklington 1895; Levy & Forsdyke 1928) and plane sinusoidal wave (Thomson 1880) have been known. Only in the past few years has it been recognized that vortex flows are one class of fluid motion which can support axisymmetric solitary waves of depression or expansion, depending on the flow configuration (Benjamin 1967(*a*); Pritchard 1970; Leibovich 1970; among others), although it had been realized earlier that long waves, a useful ingredient for solitary wave description, were possible (Squire 1962). More recently a different class of solitary-wave solution was described (Hasimoto 1972; Kida 1981) in which the waves are non-axisymmetric kinks and are described by the solution to the nonlinear Schrödinger equation, at least in the localized-induction-equation (LIE) approximation with constant L/σ, where L is an 'induction' length along the vortex and σ a measure of the core radius (see Batchelor 1967; Arms & Hama 1965; Betchov 1965). In this case, envelope solitons of constant torsion are possible solutions, a shape shared by the waves which arise in a large number of physical systems, e.g. deep-water surface waves (Yuen & Lake 1975). Moore & Saffman (1972), who modified Crow's (1970) 'cut-off' theory, showed that the dispersion relationship for a train of helical waves depends, in fact, on the vortex structure and also by inference that the induction length L of the LIE depends on the wavenumber. This important conclusion has also been demonstrated in a recent work by Leibovich & Ma (1983). Here we are able to extend the Moore–Saffman results to waves of all wavelengths by modifying a result due to Pocklington (1895), for hollow-core vortices, to include a wide range of core structures. It will be seen that the properties of solitary waves are profoundly affected by the use of dispersion relationships which take into account details of vortex structure instead of the simplest assumption of constant L/σ used by Hasimoto (1972), a point we discuss in some detail.

While some parts of this theoretical framework have already been subject to a certain amount of experimental scrutiny, in particular stationary axisymmetric waves on supercritical core flows, the so-called vortex-breakdown phenomenon (Harvey 1962; Sarpkaya 1971; Garg & Leibovich 1979; Escudier, Bornstein & Maxworthy 1982), others have not. Here it is part of our programme to look, mainly, at non-axisymmetric wave phenomena, to describe their properties and then use them to understand the results of HBG.

In §2 we describe the apparatus. The measured undisturbed vortex structure for different suction rates is presented in §3. The results of the torsional wave motions (helicoidal, plane and kink wave) are described in §4, and discussed in the context of HBG and the Hasimoto (1972), Moore & Saffman (1972), Pocklington (1895) and Leibovich & Ma (1983) theories in §5. In §6 we present new theoretical results on the solitary-wave properties of the Pocklington dispersion relationship. In §7 we highlight some properties of axisymmetric travelling waves. Finally (§8), we discuss the application of these observations to the wave motions described in HBG and seen in new sequences taken from their photographic records.

Although there now appears to be no direct relation between concentrated vortex formation in a turbulent system and the wave motions upon them, we think it useful to discuss, in the Appendix, a possible mechanism by which we believe concentrated, cyclonic vortices are formed when a turbulent field is subjected to a rotational constraint. By this mechanism vortex concentration and consequent wave motions upon them are possible occurrences in a variety of real systems.

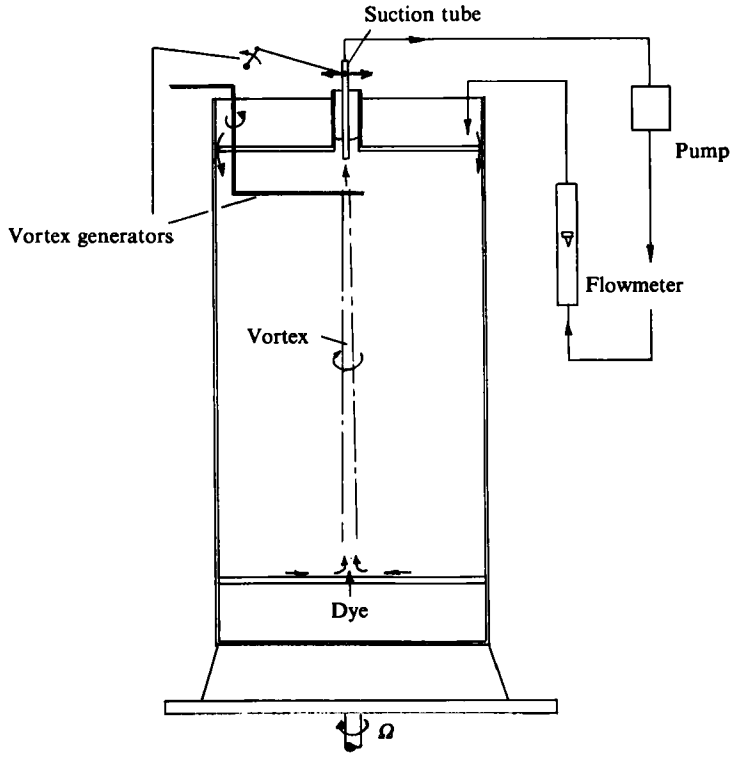

FIGURE 1. Apparatus. A suction tube within a rotating tank creates a convergence of vorticity towards the centreline and forms a concentrated vortex. This vortex can be disturbed by shaking the tube horizontally, by cutting the vortex with the thin-wire disturbance generator or by suddenly stopping the suction for a short time interval. The suction-tube diameter is 1.27 cm.

2. Apparatus and experimental procedure

The basic apparatus is identical to that used in HBG, except that the grid mechanism was replaced by a plastic plate and an apparatus to produce a single concentrated vortex was mounted within and around the tank (figure 1). The latter consisted of a central suction tube of 1.27 cm diameter connected to a pump, flowmeter and discharge pipe all mounted outside the tank on a framework sitting on the laboratory floor. The vortex was made visible either by injecting dye through a central hole in the bottom plate or by observing the trajectories of small neutrally buoyant particles circulating through the system. The latter were used to measure the axial and swirl velocity profiles within the vortex. After several initial trials, three flow conditions were chosen, all had the same clockwise† (positive) tank rotation rate $\Omega = 1.51$ rad/s with three different total flow rates 130, 180 and 230 l/h.

The vortex was perturbed in three different ways. Initially, to produce isolated kink waves, a thin metal rod was swung horizontally so that it cut the vortex at either the top or the bottom (or both in some cases). This had the effect of both stopping the vertical flow in the cut section for an instant and also of bending the core. A second, cleaner, method of producing reproducible helicoidal or standing waves was to oscillate the suction tube by a crank mechanism. To produce the strongest disturbances, we should have oscillated the tube in a circular motion in the sense

† Looking down on the rotating tank.

opposite to the basic vortex rotation. Since this was hard to do in the present case, the tube was oscillated in a plane, which produced acceptable though not optimal disturbances. Finally, axisymmetric waves could be produced by stopping the exit flow for a short time (typically 0.1 s) and allowing the initial perturbation to develop into a sequence of solitary waves. On restarting the flow the vortex immediately reformed by propagating a wave of contraction along the vortex core.

3. The measured undisturbed flow field

The undisturbed flow field of the vortex at the middle of the tank is shown in figure 2, in non-dimensional form, for the three cases considered. The vortex model to which we compare the measured velocity profiles is the Burgers vortex given by

$$\frac{V}{V_{\mathrm{m}}} = 1.39[1-\exp(-1.28r^{*2})]/r^{*} \tag{1a}$$

and

$$\frac{W}{W_{\mathrm{m}}} = \exp(-0.54r^{*2}) \tag{1b}$$

where $r^{*} = r/r_0$ and W_{m} the maximum axial velocity. The coefficients have been obtained from a least-square fit of the model to the case $Q = 230$ l/h with $r_0 = 0.33$ cm corresponding to the position where $V = V_{\mathrm{m}}$. This is also a good fit for the other two cases, except that it underestimates somewhat the vorticity at large r. This is seen from figure 3, showing the vorticity distribution for the three cases studied. The variance in the experimental points of the axial vorticity near the core centre is not surprising in view of the difficulty in measuring the velocity distribution in the vortex at small r/r_0. The azimuthal vorticity component calculated from the velocity field given by (1*b*), which is a good representation of the axial velocity (figure 2), is also shown in figure 3. Its contribution is less than 10% of the core vorticity, and in all the following discussions we neglect this component of the vorticity.† The circulation obtained from the Burgers model, adjusted to the experimental velocity data, is related to the maximum velocity and r_0 by

$$\Gamma = 1.39(2\pi r_0 V_{\mathrm{m}}). \tag{2}$$

The vortices are relatively thick, with a radius to the maximum velocity of approximately 0.33 cm, a value which varied slightly with flow rate, but, as is seen from figure 2, this variation is negligible for practical purposes (0.31 cm $\leqslant r_0 \leqslant$ 0.34 cm). In a later series of qualitative tests, the core was made much thinner by inserting a porous plate on the bottom of the tank and withdrawing fluid from the bottom boundary layer. This greatly modified the boundary-layer eruption and vortex breakdown at the bottom of the tank and created a thinner initial core diameter as a bottom boundary condition on further core development (Maxworthy 1972). However, this scheme gave a rather unsteady core, owing to pore blockage and the small diameter of the porous plate, and was not used in the reported wave experiments.

The vorticity distribution shown in figure 3 indicates that a considerable amount of vorticity lies outside any reasonably defined core radius (e.g. the radius r_0 at which V is a maximum). For many years theories to describe vortex motion assumed that the core was thin compared with some reference length (e.g. the wavelength of a

† The radial component due to tapering of the vortex is very small.

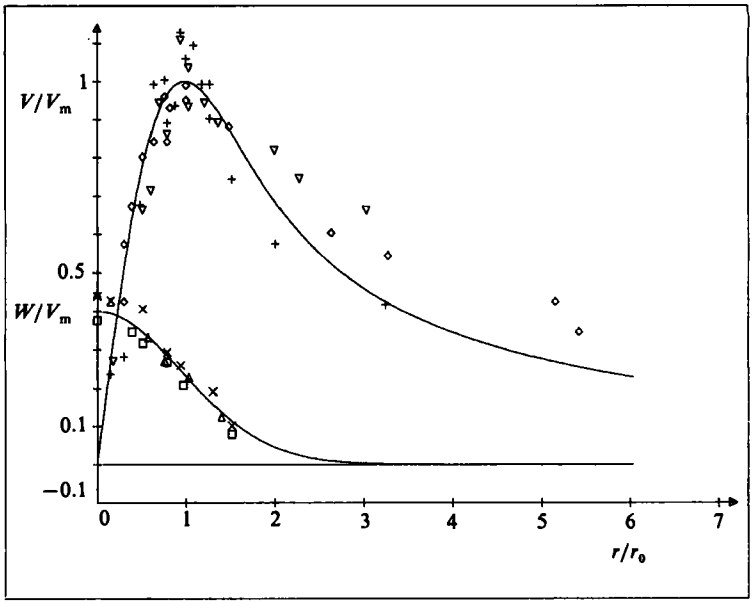

FIGURE 2. Undisturbed swirl and axial velocity profiles for the three cases considered in this paper, $\Omega = 1.51$ s^{-1}: ▽, △, flow rate $Q = 130$ l/h, $V_m \simeq 58$ cm s^{-1}, $W_m \simeq 25$ cm s^{-1}: ◇, □, 180 l/h, 93 cm s^{-1}, 35 cm s^{-1}: +, ×, 230 l/h, 132 cm s^{-1}, 58 cm s^{-1}. ——, calculated from (1*a*, *b*), adjusted for the case $Q = 230$ l/h; the core radius $r_0 = 0.33$ cm.

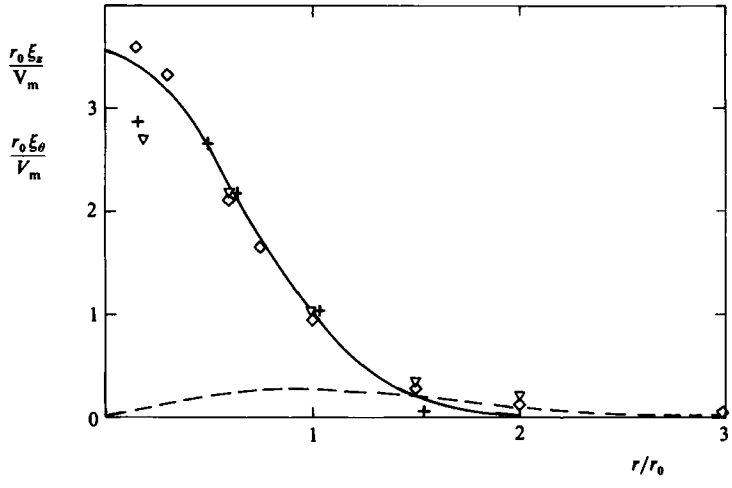

FIGURE 3. Axial and azimuthal components of vorticity plotted as functions of non-dimensional radius. The vorticity has been calculated from locally smoothed velocity profiles. Symbols refer to the same conditions as in figure 2. ——, axial vorticity component calculated from $r_0 \xi_z / V_m = 3.56 \exp(-1.28 r^{*2})$; ---, azimuthal vorticity component calculated from $r_0 \xi_\theta / V_m = 1.08 r^* \exp(-0.54 r^{*2})$. Note that the radial component and the background rotation are negligible.

typical disturbance) and that all of the vorticity was contained within it. At the heart of these approximations lies the 'localized-induction equation' (LIE) most explicitly described by Arms & Hama (1965) (see Batchelor 1967, p. 509), in which the induced velocity at any point on the vortex centreline is due only to the vorticity in these elements within a short distance L, on either side of the point. The ratio of L to some

characteristic vortex-core radius σ is to first-order approximation assumed to have some constant value, which as far as we know has only been estimated for a small number of examples: for vortex rings (with constant curvature), where it turns out to depend on at least the Reynolds number (i.e. effective vortex-core diameter) (Sallet & Widmeyer 1974), and for the one case of a kinked solitary wave by HBG. In the cases we consider in §4 we are able to estimate this quantity and show how it varies, not only with the vorticity distribution, but also with the curvature of the filaments produced in our experiments. Only recently have attempts been made to take account of the structure of the basic vorticity found in practice (Crow 1970; Moore & Saffman 1972; Leibovich & Ma 1983), and we show in §5 how the results of Moore & Saffman and an extension of the Pocklington (1895) theory can explain our experiments very well.

4. Properties of torsional waves

4.1. *Helical waves of constant amplitude*

The helical wave on a vortex filament was first discussed by Levy & Forsdyke (1928), who calculated both its steady motion and stability. Subsequently, the results have been rediscovered by Betchov (1965) and Kida (1981). To the degree of approximation appropriate to most of our results, for which the ratio of helix wavelength λ to core displacement a is very large, the speed of propagation of the wave form, or wave crest, is given, in the LIE approximation, by

$$C_{\mathrm{p}} = \frac{\Gamma}{4\pi} \frac{k}{(1+k^2a^2)^{\frac{1}{2}}} \ln \frac{L}{\sigma} \approx \frac{\Gamma k}{4\pi} \ln \frac{L}{\sigma}, \tag{3}$$

so that the dispersion relationship becomes

$$\omega \approx \frac{\Gamma k^2}{4\pi} \ln \frac{L}{\sigma}, \tag{4}$$

where ω is the wave frequency, $k = (2\pi/\lambda)$ is the wavenumber and Γ is the circulation around the vortex core. We also note for future reference that the wave curvature is given to the same degree of approximation by

$$\kappa \approx 4\pi^2 \frac{a}{\lambda^2} = k^2 a. \tag{5}$$

In figure 4(*a*) we show a photograph of a helical vortex filament produced by oscillating the suction tube at a fixed frequency starting from rest just a short time before the picture was taken. The leading edge of the wavetrain is propagating into an undisturbed region followed by a more-or-less regularly oscillating core. Tracings of the vortex centre of a sequence of such waves at equal time intervals are shown in figure 5, where we have drawn the progress of each wave trough and crest. In these cases with the undisturbed vortex rotating in the clockwise direction, when looking from above, the helix is right-handed and is rotating in a counterclockwise direction and the phase of the waves propagates downwards. We can then use the velocities represented by these lines, corrected for the effect of tank rotation, to calculate L/σ in (3). To do this we have to decide on a value for Γ. Using the most obvious value, namely that at the value of radius where V is a maximum, gave values for L/σ which were both a function of flow rate and a function of the curvature of the wave as measured by κr_0. Good data collapse to a single curve was found by using the value

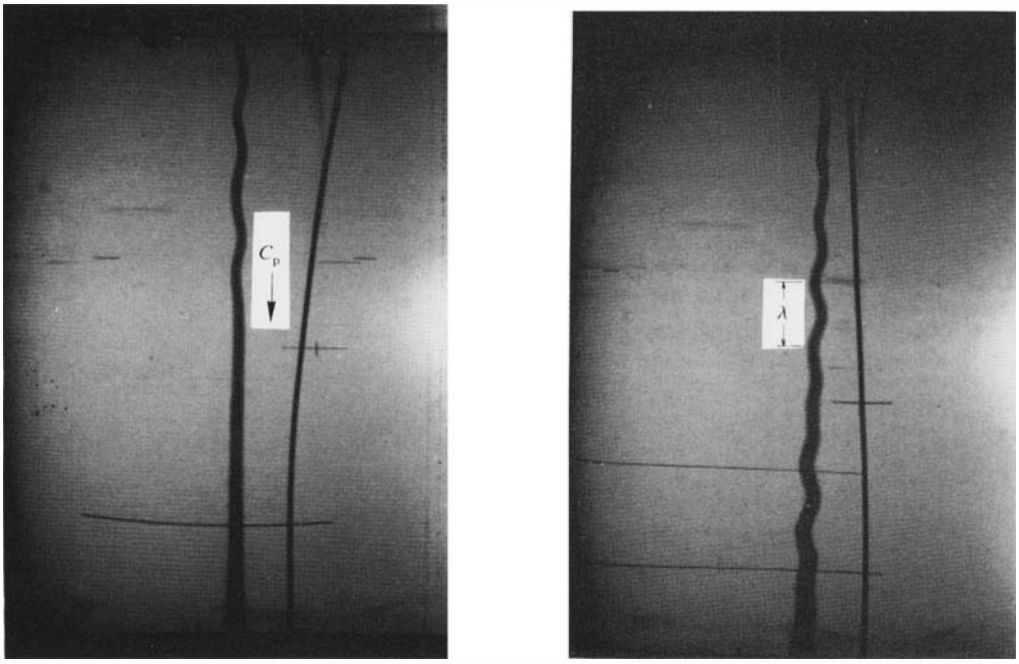

FIGURE 4. Photographs of (*a*) a helical vortex filament wave (the maximum and minimum wave amplitude are propagating downwards); (*b*) a standing wave. The wavelength is fixed while the pattern rotates without propagation of phase. The dark lines running down the tank next to the vortex filaments are dye supply tubes.

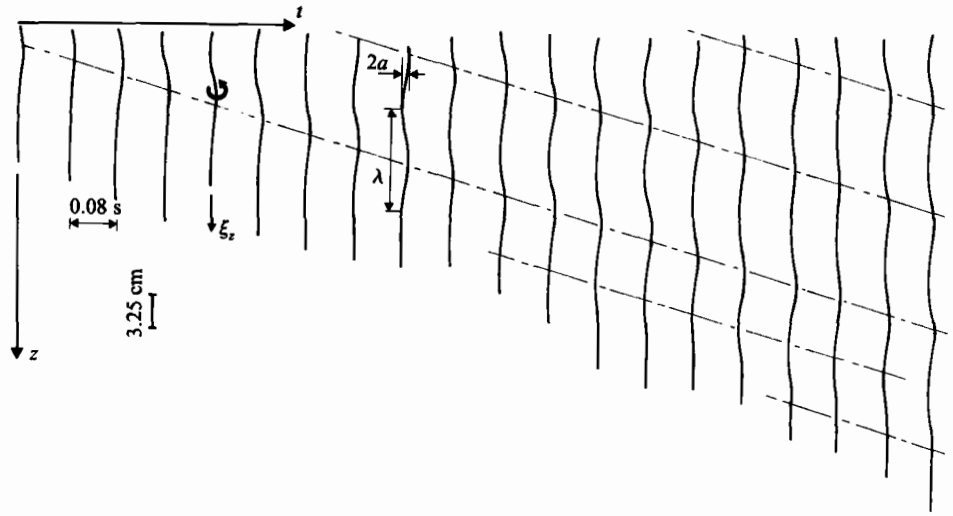

FIGURE 5. Tracings of the vortex centreline of sequences of helical waves as a function of time showing the progress of each wave crest for the case $Q = 180$ l/h. Oscillation frequency of suction tube $n = 1.6$ rad s^{-1}, giving $\lambda = 10.8$ cm, $a = 0.4$ cm and $C_p = 17.2$ cm s^{-1}. The chain-dotted lines indicate lines of constant phase. Note that the rotation of the vortex filament indicated by ↻ is opposite to the sense of the vorticity of the undisturbed vortex.

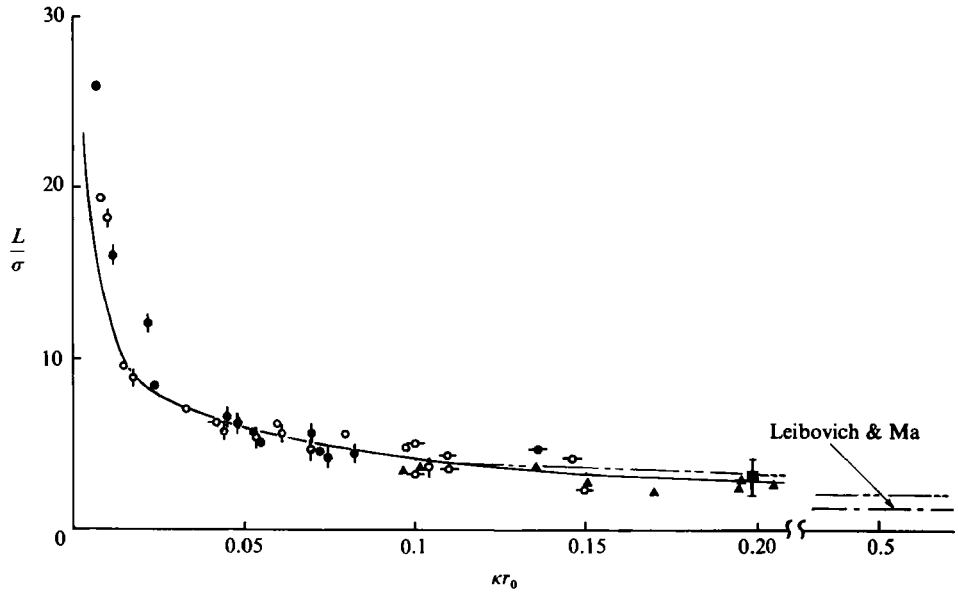

FIGURE 6. L/σ versus κr_0 or $k^2 a r_0$ for all of the cases considered in this paper. ●, ◐, ◉ travelling helical waves; ○, ◌ ⊖, standing sinusoidal waves; ▲ solitary kink waves. The point ■ is from HBG. ——, Moore & Saffman relation with $F = -0.45$. The chain-dotted line is the value of L/σ given by Leibovich & Ma (1983) for the range $0.46 \leqslant \kappa r_0 \leqslant 1$ and the double chain-dotted line is the modified Pocklington relationship.

of Γ calculated at twice the radius of the maximum velocity. From figure 3 it is seen that at $r/r_0 = 2$ the vorticity has dropped to about 5 % or less of its maximum value, so that the circulation at $r/r_0 = 2$ approximates the vortex circulation to within experimental error. The resulting curve of L/σ versus κr_0 is shown in figure 6 with values for the experiments discussed in §5 also included, although they, being more accurate, were actually found first. The actual values of Γ used in calculating L/σ shown in figure 6 were 330, 300 and 184 $\mathrm{cm^2\,s^{-1}}$ for $Q = 230$, 180 and 130 l/h respectively. These values differ somewhat from those given by the Burgers model (2), which would give 299, 267 and 168 $\mathrm{cm^2\,s^{-1}}$ respectively. The most striking observation is that L/σ is a strong function of κr_0, a result which is discussed in detail in §5, with further implications presented in §§6 and 8.

The other interesting result which can be seen by reference to figure 5 is that more waves exist at the end of the sequence than were put in by the oscillation of the upper end of the filament. Since wave energy appears to propagate faster than the phase of the waves, the group velocity of this dispersive wavetrain must be greater than the phase speed – a point we discuss in detail in §5.

4.2. *Standing waves*

When the downward-propagating helical wave described above reflects from the bottom boundary, it is transformed into a left-handed screw also rotating counterclockwise. The interaction of these two waves produces a plane standing wave (i.e. a wave with no torsion which does not propagate), also rotating counterclockwise. This is the classical wave motion described originally by Thomson (1880) and most readily available in Batchelor (1967, p. 511).

The pattern rotates so that the points of maximum excursion from the centreline rotate with a velocity

$$\omega_p a_m = -\Gamma\pi \frac{a_m}{\lambda^2} \ln \frac{L}{\sigma}, \tag{6}$$

where λ is again the wavelength and a_m the maximum radial excursion of the core centreline.

However, this velocity also equals $2\pi a_m n$, where n is the frequency of oscillation of the vortex in cycles/s. Equating these two results gives

$$\frac{L}{\sigma} = \exp\left\{\frac{2\lambda^2 n}{\Gamma}\right\}, \tag{7}$$

so that in this case the calculation of L/σ is reduced to the measurement of the wavelength produced in response to an oscillation of known frequency.

In figure 4(*b*), we show a photograph of such a standing wave for the conditions given in the caption. On figure 6 we have included the values of L/σ calculated from (7) again versus κr_0 or $k^2 a_m r_0$, where κ is the same as (5) for large λ/a_m.

4.3. *Isolated kink waves*

We have refrained from calling this subsection 'solitary kink waves' because it now appears that the waves we can produce most readily are not solitary waves in the classical sense (see §§6 and 8). They are evolving during our observations, but they do seem to exhibit some of the features of solitary waves. We start our discussion with a description of the formation process. In the first method the suction tube was oscillated quickly through one cycle and the evolution of the resultant single kink followed photographically. In the present apparatus, such waves were of such small amplitude, compared to the visible core size for example, that it was impossible to obtain any useful information from them. Alternatively, and first chronologically, the core region at either the top or bottom could be disturbed by rapidly cutting through the core with a thin solid rod. This had effects which were different depending on the direction of propagation.

When the core was cut near the top, the axial flow was cut off briefly, and this information was transmitted to the rest of the vortex by an axisymmetric solitary wave of expansion, which, depending on its amplitude, sometimes became unstable and produced growing spirals behind it. This axisymmetric wave had a high velocity and rapidly left the region of the original disturbance. A second perturbation was created by the motion of the rod and this consisted initially of a single kink under most circumstances (see figure 7). At the same time as this kink began to propagate, the axial flow was reestablished by a wave of contraction or convergence from the suction tube, which also had a much higher velocity than that of the kink. In figure 8(*a*) we show the evolution of a typical kink of this type. The chain-dotted lines join identical points on the pattern in a frame of reference moving with the envelope or group velocity, while the dotted line joins the positions of a wave crest. Owing to the small differences in these speeds, the waves appear to enter the front of the envelope, travel slowly through it and leave from the rear. Alternatively the pattern appears to rotate slowly clockwise, that is, in the sense of the vortex flow. As in the case of the helical wave, new waves appear ahead of the old crests owing, as we will show, to the higher group velocity. This effect confused interpretation of the wave pattern at first, since if one was not careful in following the developing wave, the pattern appeared to rotate in the wrong direction. A close examination of the

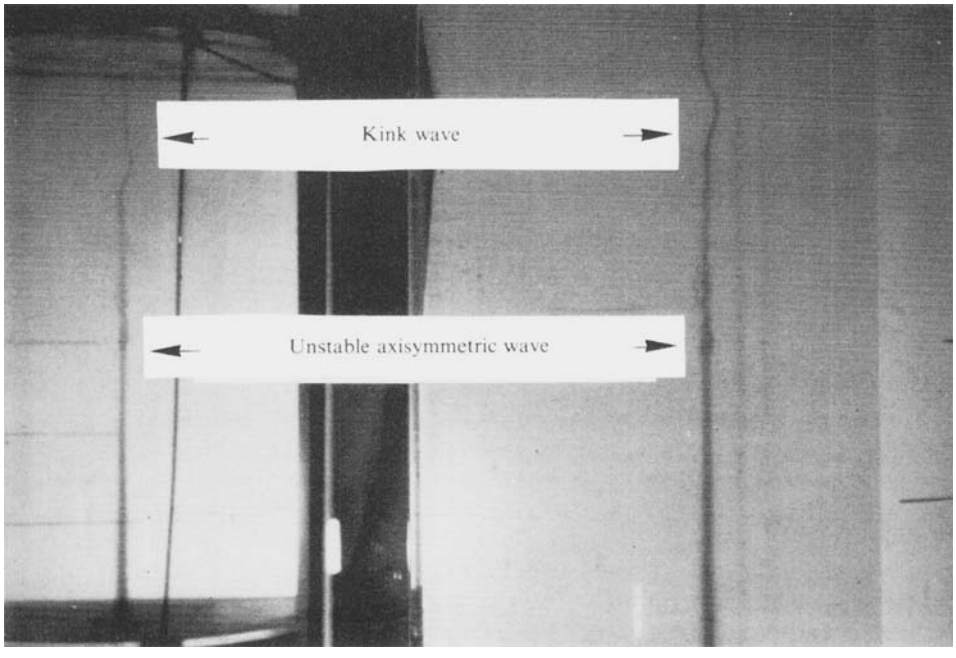

FIGURE 7. Photograph of an isolated kink wave produced by cutting the core at the top. The unstable axisymmetric wave produced at the same time, by briefly stopping the axial flow when the rod moves through the vortex, is also visible. The view of the left-hand side is a 90° mirror image. The dark line seen in the mirror image next to the vortex filament is a dye supply tube.

wave velocities showed that both the group and phase velocities decreased slightly as the wave propagated. This is clearly seen from the dotted line drawn through the wave crests in figure 8(*a*) which indicates a decrease of the phase velocity by about 10 % during the time of observation. The wave pattern velocity has a lesser variation and since in addition the wave pattern envelope is less well defined, we have represented its displacement by a straight line in figure 8(*a*). This decrease in wave speeds can be explained by the slight increase in wavelength over the trajectory (see below). Furthermore, we will see from the discussion in §5 (see also figure 9) that for waves on a real vortex the phase velocity decreases relative to the group velocity when the wavenumber decreases. In figure 8(*b*) we have indicated what happens when the wave interacts with the endwall. The wave goes through a phase advance as it does so and reappears as a left-handed kink. Similar head-on interactions between waves travelling in opposite directions are presented in Maxworthy, Mory & Hopfinger (1983), and show a similar phase advance which is characteristic of solitary-wave interactions.

At first we attempt to analyse our results using the only available and complete theory – that of Hasimoto (1972) as interpreted by HBG and extended below. In this theory, in which, critically, L/σ is assumed constant, the speed of the wave envelope, which is the group velocity, is given by

$$C_g = 2\tau_0 \frac{\Gamma}{4\pi} \ln L/\sigma, \tag{8}$$

where τ_0 is the wave torsion, which for small a_m/λ is approximately equal to $2\pi/\lambda$,

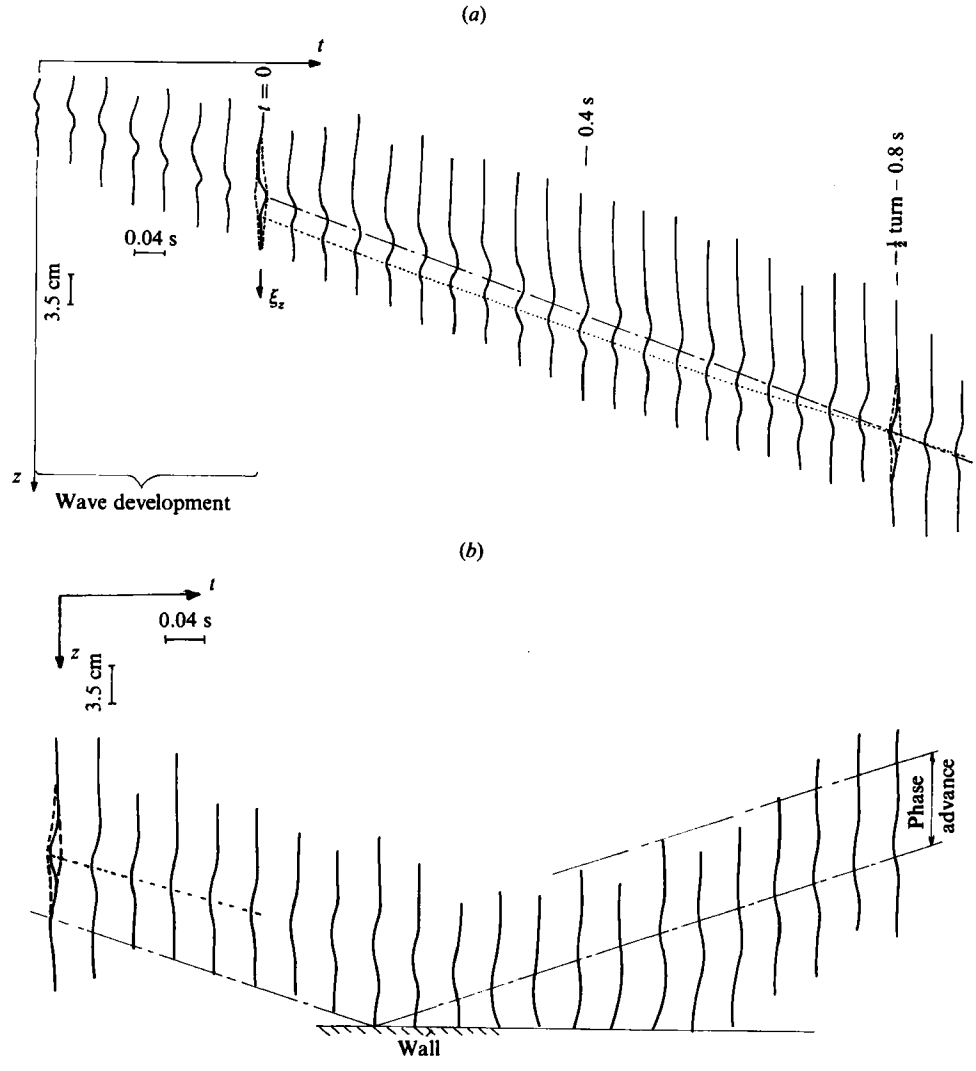

FIGURE 8. Tracing of the vortex centreline of the time evolution of an isolated kink wave for the condition $Q = 180$ l/h. (*a*) Freely propagating kink-wave; the single chain-dotted line indicates the trajectory of the estimated centre of the wave pattern moving at $C_g \approx 33$ cm s^{-1}, while the dotted line joins the positions of a particular wave crest. Note that new kinks are being formed ahead of the basic pattern. (*b*) Reflection from a boundary. It is difficult to follow individual phases through the interaction, but it is clear that the reflected wave suffers a phase advance.

where a_m is the maximum radial displacement of the core centreline and λ the wavelength of the central kink so that

$$C_g \approx \frac{\Gamma}{\lambda} \ln L/\sigma = \frac{\Gamma}{2\pi} k \ln \frac{L}{\sigma}. \tag{9}$$

However, the wave peaks move at a different speed, which can be calculated to the present degree of approximation as in (3) by noting that the rotation rate of the coils or vortex filament is given by (when $(\kappa/2\tau_0)^2 \ll 1$)

$$\omega_p \approx -\frac{\pi}{\lambda^2} \Gamma \ln L/\sigma, \tag{10}$$

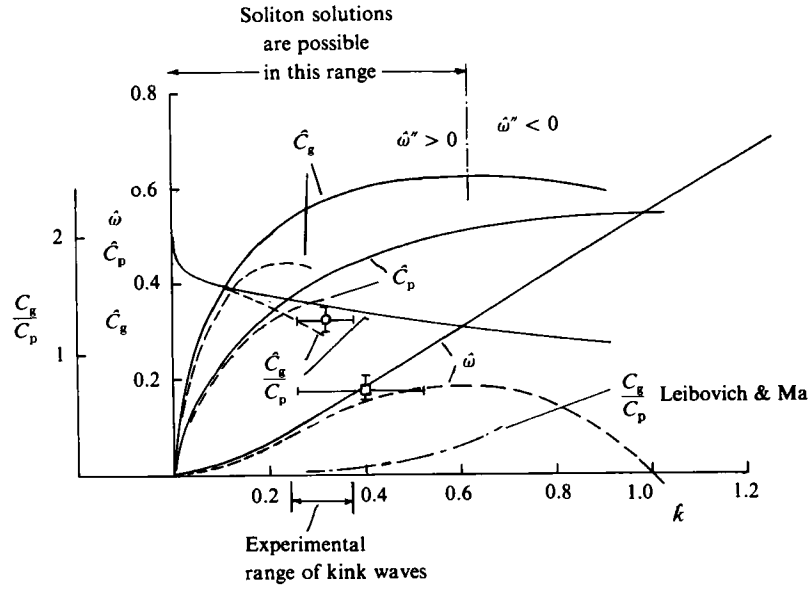

FIGURE 9. Properties of the Pocklington (1895) (——) and Moore & Saffman (1972) (– – –) dispersion relationships plotted in universal coordinates. Note that the maximum of group velocity $\partial^2\hat{\omega}/\partial\hat{k}^2$ is at $\hat{k} = 0.61$ and the fact that the Hasimoto (1972) limit $C_g/C_p = 2$ only occurs for waves of very long wavelength. Solitons obeying the nonlinear Schrödinger equation, with a single frequency carrier, can only exist in the interval $0 < \hat{k} < 0.61$. — · —, ratio of group velocity to phase velocity (C_g/C_p) obtained by Leibovich & Ma; ○, typical value of C_g/C_p from present experiments; □, C_g/C_p from HBG.

as for the helical waves (the negative sign indicates rotation opposite to the vortex flow).

The maxima and minima then appear to move at a speed $C_p = \omega_p \lambda/2\pi$, which becomes

$$C_p \approx \frac{\Gamma}{2\lambda} \ln \frac{L}{\sigma} = \frac{\Gamma}{4\pi} k \ln \frac{L}{\sigma}, \tag{11}$$

which is equal to half the group velocity and is the same as that for a train of waves (3). We note that the use of this relationship to calculate L/σ does not depend on our kink waves being solitary waves. We are, essentially, treating them as the individual waves of a longer wavetrain. The individual particles of the core do not translate, however, the effect being the same as observing the peaks of a solid screw thread as it is rotated but not translated. Thus, in a frame of reference moving with the wave envelope, the waves appear to enter the front of the packet and then propagate backwards, or alternatively appear to rotate in a direction opposite to that given by induction arguments, at a rate

$$\omega_p' \approx \frac{\pi}{\lambda^2} \Gamma \ln \frac{L}{\sigma}. \tag{12}$$

In this case the parameter used by HBG becomes

$$\frac{C_g}{\omega_p' a_m} \approx \frac{\lambda}{\pi a_m} = T, \tag{13}$$

which agrees in magnitude with their discussion, but is of opposite sign from that found here and in Hasimoto (1972). For any particular set of experiments, we measure λ and the speed of the wave peaks, and then through the use of (11) calculate L/σ.

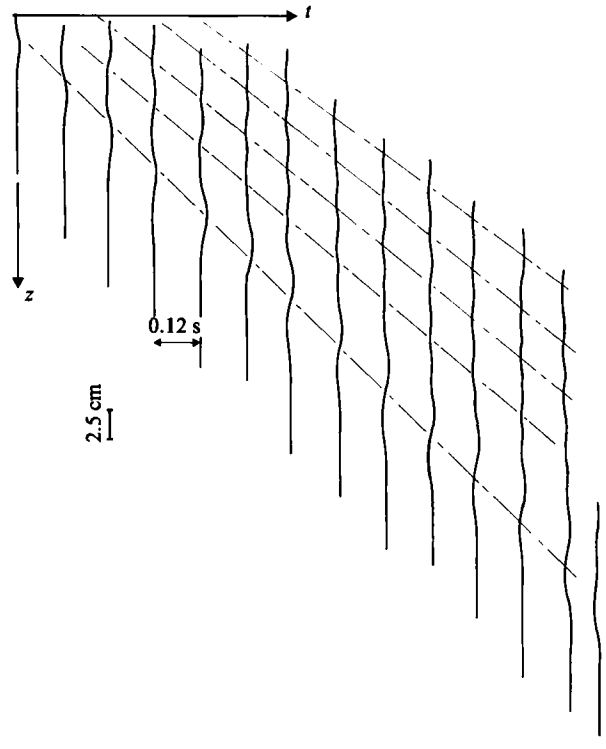

FIGURE 10. Disturbance produced occasionally by the wire cutting through the vortex core near the suction tube. Conditions $Q = 180$ l/h. A vortex kink moves at $C_g \approx 30$ cm s^{-1} ahead of a train of decaying vortex waves with a lower velocity indicated by the constant phase lines.

The points calculated in this way are also shown in figure 6 with the symbol ▲. Because of the difficulty in deciding the position and orientation of the wave at small amplitudes and long wavelengths, only waves with relatively large values of κr_0 were used. In these cases the maximum value of κ was used to plot the points on figure 6, and λ was multiplied by a small (1.05–1.01) experimentally determined correction factor to account for the fact that a_m/λ was typically of order 0.1–0.05 and κ therefore somewhat smaller than the value given by (5). One can see in figure 6 that the results for the isolated kinks form a logical extension to the existing points for helical and standing waves. This is probably not so surprising, since the evolving kink wave can be thought of as a perturbed helical wave of slightly varying wavelength and amplitude. We also note, in passing, that the two competing effects that give the observed wave speed, that is κ and L/σ, combine in such a way that over the range considered in the experiments C_p was virtually constant at 27–30 cm/s for the case where $Q = 180$ l/h for example.

We also note from figure 8 that the pattern appears to rotate slowly backwards at approximately 2.4 rad/s (referred to the rotating frame), or alternatively that the wave envelope had a velocity only slightly larger than that of the individual wave peaks, an effect that was generally true for all kink waves observed under the present experimental conditions. From our previous discussion, it is clear that this result does not agree with the predictions of Hasimoto's theory, which requires a velocity difference of a factor of about two or a much larger apparent rotation rate than that measured. These observations are rationalized in §§5, 6 and 8.

Although the vortex response to the major distorsion created by the 'cutting' rod

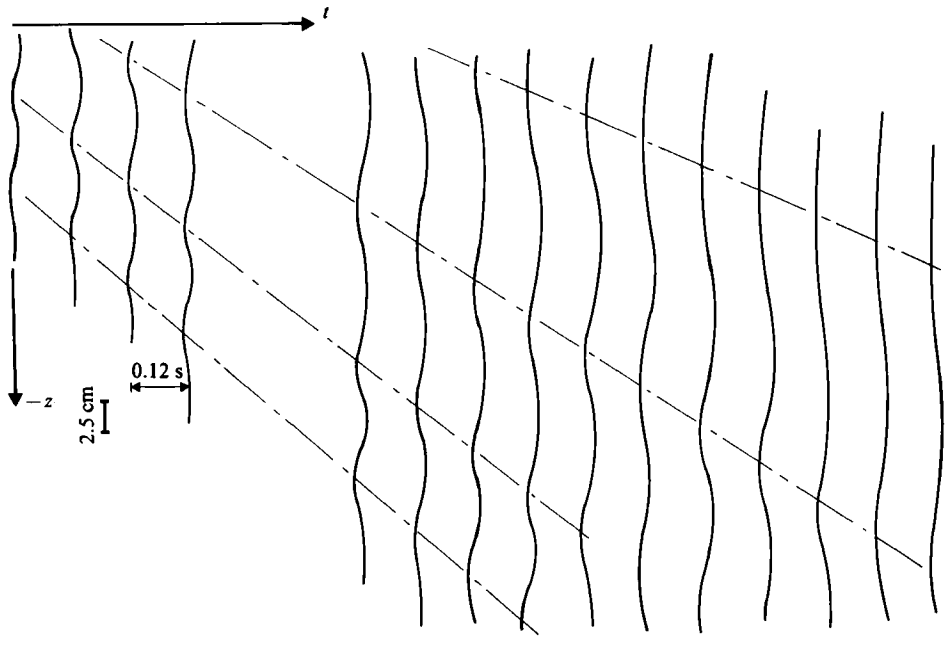

FIGURE 11. Wave shape sometimes produced by the wire disturbance generator at the bottom of the tank consisting of a train of waves of growing wavelength and almost-constant amplitude. Conditions $Q = 200$ l/h. The velocity of each wave crest is approximately constant.

was often of the type shown in figure 8, sometimes a different perturbation was formed. This appeared to consist of an isolated kink wave followed by a slowly decaying wavetrain of almost constant wavelength. In figure 10, we show a drawing of this configuration.

When the core was cut at the bottom, a rather different sequence of events took place. Immediately some form of axisymmetric disturbance moved very quickly up the core. It was, in fact, of such a small amplitude and high velocity that it could not be resolved photographically. Trailing behind was a very distinctive waveform, which can best be described as a wiggle of growing wavelength and virtually constant amplitude. A drawing of the shape of the vortex axis is shown in figure 11. Unfortunately, two frames were usually obscured by the vertical dye-supply tube in each sequence observed. The velocity of each maximum is almost constant, except as the wavelength variation becomes extreme towards the end of the observations, this being the result of the competing effects of variable κ and L/σ, which combine in such a way to give an almost constant phase speed.

5. Discussion of the experimental results

The most important results of this study are presented in figure 6, where at first we show, in the context of the LIE, that L/σ is a strong function of wave curvature κ, or alternatively the wavenumber k. We have chosen to present our results this way to show decisively the major error induced by assuming a constant value of L/σ in the calculation of filament motion and at the same time show the relationship of our results to the dispersion relationship of Moore & Saffman (1972) and a modification of Pocklington's (1895) expression for hollow-core vortices.

We motivate our final result as follows. Moore & Saffman (1972) give an asymptotic formula for helices of long wavelength:

$$\omega = \frac{\Gamma k^2}{4\pi}\left\{\ln\frac{2}{kr_0}+F\right\}, \tag{14}$$

where

$$F = \frac{1}{\Gamma^2}\int_0^{r_0}\frac{\Gamma(r)}{r}\,\mathrm{d}r - \frac{8\pi^2}{\Gamma^2}\int_0^{r_0} rW^2(r)\,\mathrm{d}r - \gamma; \tag{15}$$

$W(r)$ is the distribution of axial velocity within the core and $\gamma = 0.5772$ is Euler's constant. Letting $k^* = kr_0$, (14) becomes

$$\omega^* = \frac{4\pi\omega r_0^2}{\Gamma} = k^{*2}\ln\frac{\mathrm{e}^{F'}}{k^*}, \tag{16}$$

where $F' = F + \ln 2$.

Equation (16) is plotted on figure 9 using universal coordinates $\hat{\omega} = \omega^*\mathrm{e}^{-2F'}$ and $\hat{k} = k^*\mathrm{e}^{-F'}$ so that all dispersion relationships for all values of F fall on a single curve.

As far as we are aware, only one dispersion relationship has been calculated that is valid for all wavenumbers. This is due to Pocklington (1895), who found that for hollow-core vortices, i.e. $W(r) = 0$, and all the vorticity concentrated at a vortex sheet at $r = r_0$,

$$\omega^* = 2\left[1 \pm \left\{1 + k^*\frac{K_0(k^*)}{K_1(k^*)}\right\}^{\frac{1}{2}}\right], \tag{17}$$

where K_0 and K_1 are the modified Bessel functions.

The long-wavelength asymptotic form of (17) for the slow wave (taking the negative sign) is, in dimensionless form,

$$\omega^* = k^{*2}\left\{\ln\frac{2}{k^*} - 0.5772\right\}, \tag{18}$$

which also agrees precisely with the Moore–Saffman result (14) and (16) when one evaluates (15) for the hollow-core vortex ($W(r) = \Gamma(r) = 0$ for $r < r_0$).

Therefore one can plot Pocklington's relationship on figure 9, again using our universal coordinates and substituting $F'_{\mathrm{P}} = \ln 2 - 0.5772$, whence

$$\hat{\omega} = \omega^*\mathrm{e}^{-2F'_{\mathrm{P}}} = 2\,\mathrm{e}^{-2F'_{\mathrm{P}}}\left[1 \pm \left\{1 + \mathrm{e}^{F'_{\mathrm{P}}}\hat{k}\frac{K_0(\mathrm{e}^{F'_{\mathrm{P}}}\hat{k})}{K_1(\mathrm{e}^{F'_{\mathrm{P}}}\hat{k})}\right\}^{\frac{1}{2}}\right], \tag{19}$$

where in this case $\hat{k} = k^*\mathrm{e}^{-F'_{\mathrm{P}}}$. In figure 9 we can see that Moore–Saffman is a true asymptote to the Pocklington curve but that several important differences do exist. Of critical importance to the discussion of §6 is the fact that the change in sign of $\mathrm{d}^2\omega/\mathrm{d}k^2$, i.e. $\mathrm{d}C_{\mathrm{g}}/\mathrm{d}k = 0$, occurs at shorter wavelengths for the Pocklington curve than for Moore–Saffman and that neither C_{p} nor C_{g} become zero.

For future reference the phase velocity becomes

$$\hat{C}_{\mathrm{p}} \equiv C^*_{\mathrm{p}}\,\mathrm{e}^{-F'_{\mathrm{P}}} \equiv \mathrm{e}^{-F'_{\mathrm{P}}}\frac{4\pi r_0 C_{\mathrm{p}}}{\Gamma} = \frac{2}{\hat{k}}\,\mathrm{e}^{-2F'_{\mathrm{P}}}\left[1 \pm \left\{1 + \mathrm{e}^{F'_{\mathrm{P}}}\hat{k}\frac{K_0(\mathrm{e}^{F'_{\mathrm{P}}}\hat{k})}{K_1(\mathrm{e}^{F'_{\mathrm{P}}}\hat{k})}\right\}^{\frac{1}{2}}\right] = \frac{\hat{\omega}}{\hat{k}} \tag{20}$$

and the group velocity becomes

$$\hat{C}_{\mathrm{g}} \equiv C^*_{\mathrm{g}}\,\mathrm{e}^{-F'_{\mathrm{P}}} \equiv \mathrm{e}^{-F'_{\mathrm{P}}}\frac{4\pi r_0}{\Gamma}C_{\mathrm{g}} = \mathrm{e}^{-F'_{\mathrm{P}}}\left\{\frac{\pm\left[\dfrac{2K_0}{K_1} + \mathrm{e}^{F'_{\mathrm{P}}}\hat{k}\left(\dfrac{K_0^2}{K_1^2} - 1\right)\right]}{\left[1 + \mathrm{e}^{F'_{\mathrm{P}}}\hat{k}\dfrac{K_0}{K_1}\right]^{\frac{1}{2}}}\right\}, \tag{21}$$

where $C_p = \omega/k$ and $C_g = d\omega/dk$ are the dimensional phase and group velocity respectively and we choose the slow wave (negative sign in (20) and (21)) as the appropriate branch of the relationship. As a final step we suggest that, since the asymptotic form (16) is valid for all values of F', that one can modify the Pocklington formula to be valid for values of F' close to F'_P in the following way:

$$\omega^* = 2\,e^{2F'-2F'_P}\left[1 \pm \left\{1 + e^{F'_P-F'}\,k^*\,\frac{K_0(e^{F'_P-F'}\,k^*)}{K_1(e^{F'_P-F'}\,k^*)}\right\}^{\frac{1}{2}}\right], \tag{22}$$

which is the equivalent of (17) for values of F' different from F'_P.

This has the correct asymptotic behaviour (16) as $k^* \to 0$ for all F', and will be a better approximation to the true dispersion curve than (16) for moderately large values of k^*, say up to $k^* = O(1)$.

In order to compare these results with our experimental values of L/σ, we note that within the Moore–Saffman formulation $L/\sigma = e^{F'}/k^*$, or, upon noting that $\kappa r_0 \approx k^2 a_m r_0$,

$$\frac{L}{\sigma} = \frac{e^{F'}}{(\kappa r_0)^{\frac{1}{2}}}\left(\frac{a_m}{r_0}\right)^{\frac{1}{2}}. \tag{23}$$

In our experiments $a_m/r_0 \approx 1$, and so on figure 6 we have plotted (23) for a value of $F = -0.45$. This value gives a remarkably good fit to the experimental data over the range of the experiments, and only deviates noticeably at small values of κr_0. Calculation of F based on the velocity profiles expressed by $(1a, b)$ gives a value of -0.43, where the effective core radius is taken as r_0 and Γ is the value of the circulation at $r = 2r_0$. Further calculations based directly on the measured profiles give $F = -0.46$.

In order to plot the Pocklington (1895) results on the same graph, we note that $\hat{\omega} = \hat{k}^2 \ln(L/\sigma)$ within the LIE approximation, so that $L/\sigma = e^{\hat{\omega}/\hat{k}^2}$, where the value of $\hat{\omega}$ can either be calculated from (19) for a given wavenumber k using $\hat{k} = kr_0\,e^{-F'}$, or can be taken directly from figure 8. Equivalently, since L/σ also equals $e^{\omega^*/k^{*2}}$, we can use (22) to calculate ω^* for a chosen value of $k^* = kr_0$. These values of L/σ are plotted in figure 6. We note that over the range of the experiments (22) is also a good approximation to our experimental results for $F' = \ln 2 - 0.45$ and $F'_P = \ln 2 - 0.5772$.

We see from figure 9 that, for the range of L/σ or k we observe in our experiments on isolated kink waves, C_g/C_p is greater than unity by at most 40 %, and approaches 30 % at the extreme values of κr_0 shown in figure 6. In the example of figure 8 the measured group velocity is approximately 20 % higher than the phase speed, while use of figure 9 and a mean value of 3.4 for L/σ over the wave trajectory gives a difference of about 35 %.

We can now also explain the results found for the helical waves in a similar fashion. For example, in figure 5 we noted the appearance of extra helices ahead of the first phase front. Unfortunately we cannot estimate the group velocity directly from figures such as these, since the disturbance propagating ahead of the first phase front has a somewhat smaller value of k than the waves that follow, and hence a larger value of C_g/C_p than the main wavetrain. This we observe in figure 5, where the first minimum (or maximum) propagates ahead of the wave with a velocity some 40 % larger than the phase speed, which is close to but not equal to what we would expect from the values of κr_0 within the main wavetrain.

Recently Leibovich & Ma (1983) also obtained kink-wave solutions for a vortex with a vorticity distribution of the type considered by Burgers (1948). Ultimately,

they determine a relationship between a quantity h, related to our κr_0, and L/σ. In our notation and for small core displacements,

$$\kappa r_0 \approx 2a_m/r_0 h.$$

For typical values of a_m and r_0, in our experiments, values of κr_0 correspond to values of h of order 10, in which case L/σ is typically 1.2 according to Leibovich & Ma, and does not vary very much as κr_0 is varied. The comparison plotted on figure 6 for the range of κr_0 that Leibovich & Ma (1983) determine is the one for which solitary waves can exist (see, however, §6), and this shows that their estimate may in fact asymptote to the experimental values. Their results also indicate that the grouping $\kappa r_0^2/2a_m$ would be more appropriate than our grouping κr_0, but our experiments do not cover a large enough range of a_m or r_0 to check this quantitatively. The phase speed calculated by Leibovich & Ma is always greater than the group velocity for values of κr_0 typical of our experiments. In fact, if we use their values of phase speed for helical waves in order to calculate equivalent values of L/σ, we obtain values which are at least one to two orders of magnitude larger than those found experimentally. The ratio of C_g/C_p, calculated from their figure 1, in which they give C_g and the wave frequency ω^* as functions of a dimensionless wavenumber, is indicated in figure 8 for comparison. Two interesting observations can be made: one is that in their case $C_g/C_p \to 0$ as $k \to 0$, which is in direct contradiction with our results, which agree with Moore & Saffman and two is that the ratio of C_g/C_p is much less than unity and that a Hasimoto soliton, with which they 'calibrate' their solution, does not seem an appropriate possibility under these circumstances.

The Leibovich & Ma theory, however, has in its favour that it establishes the existence of solitary kink waves for $C_g/C_p < 1$ as observed by Hopfinger & Browand (1982; see also HBG†), whereas the Pocklington dispersion relation always gives $C_g/C_p > 1$. The Moore & Saffman dispersion relation would indicate the existence of waves with $C_g/C_p < 1$, but these would most likely not be solitary waves (see §6). From HBG we find $C_g/C_p \approx 0.7$ for $L/\sigma \sim 4$ or $k \sim 0.3$. The values of Γ and σ (their ϵ) in HBG are lower bounds, and the former can easily be greater by a factor of 2, giving $L/\sigma \sim 2$ and $k^* \sim 0.6$. These bounds are shown in figure 9. The range of k^* corresponds to the range of validity of Leibovich & Ma's theory, but the value of C_g/C_p differs by an order of magnitude.

6. Comments on the theory of solitary waves obeying the extended Pocklington dispersion relationship

The possible existence of kink-wave solitons propagating along isolated vortex filaments in an otherwise irrotational fluid was first discussed by Hasimoto (1972). Starting with the Frenet–Seret formulae for a space curve, together with the LIE with constant L/σ, for the self-induction of a line vortex, Hasimoto demonstrated that the filament distortion evolves according to the cubic-nonlinear Schrödinger (NLS) equation

$$\frac{1}{\mathrm{i}}\frac{\partial \psi}{\partial t} - \frac{\partial^2 \psi}{\partial s^2} = \tfrac{1}{2}|\psi|^2\psi. \tag{24}$$

† HBG pointed out that the pattern rotation agreed in magnitude with Hasimoto's theory, but not in the sense of rotation (HBG, p. 526).

The complex wave function ψ is defined in terms of the filament curvature κ and torsion τ by the relation

$$\psi(S,t) = \kappa \exp\left\{\mathrm{i}\int^{s} \tau \, \mathrm{d}s'\right\} \tag{25}$$

and s measures distance along the vortex core. The signs of the dispersive and nonlinear terms in (24) are consistent with those required for the equation to admit envelope or wave-packet solitons solutions. Hasimoto also showed that the NLS equation (24) and the transformation (25) represented an exact reduction of Betchov's (1965) intrinsic equation for vortex motion. The linear form of (24), linearized about an undisturbed state having $\kappa = \tau = 0$, is consistent with the dispersion relation

$$\omega^* = k^{*2} \tag{26}$$

for infinitesimal helicoidal waves on a vortex within the limitations of the LIE. For this dispersion relationship, envelope solitons are possible for *all* narrow-band, carrier wavenumbers. On the other hand, when the effects of motion *within* the finite core are considered and the LIE is *not* invoked, both Pocklington (1895) and Moore & Saffman (1972) derived more appropriate relationships for helical oscillations of a vortex core, written in normalized form in (19) and (16). The appearance of the modified Bessel functions in (19) and logarithmic term in (16) has important implications for the form of the evolution equation for ψ and therefore the existence of vortex solitons. In both cases the second term in (24) is greatly modified, and assuming that the form of the nonlinear term is the same as in (24), at least to leading order, the resulting modified NLS equations have no known permanent-wave solutions.

If, on the other hand, the Pocklington dispersion relationship (19) is represented *locally* by a parabolic approximation, the evolution of a *narrow-band* wave packet is still described in terms of the NLS equation (24) with suitably modified coefficients. In this case, however, it is clear from figure 9, where the properties of (19) are sketched, that the curvature of the dispersion curve, which is the coefficient of $\partial\psi/\partial s^2$ in (24), reverses sign for wavenumbers $\hat{k}$ above or below 0.61. When $\hat{k} > 0.61$ and the curvature is negative, the signs of both the dispersive and nonlinear terms in (24) are positive, and no permanent-wave groups can exist on an otherwise straight filament. On the other hand, for $\hat{k} < 0.61$ the curvature is positive and these terms can balance to produce soliton solutions.

We note that all of our experiments were performed within this latter region and that vortex solitons were a possibility. However, we see that in figure 8, and all other similar cases, no steady-state solitary waves were ever observed. Two explanations are possible: The simpler is that the waves were still evolving towards a soliton state during our observations and that a much larger tank would be needed to observe them. Secondly, it is well known that NLS solitons are only possible if the nonlinear term exceeds a certain magnitude. For the Hasimoto soliton it is required that the maximum wave amplitude exceed $1/\pi$ times the carrier wavelength. This is certainly not true of any of our waves although the magnitude of the dispersion term is smaller within our range and hence the required nonlinearity for soliton formation is likely to be smaller also. A complete study of the type performed by Leibovich & Ma would be necessary to clarify these questions.

7. Axisymmetric waves

As we have already described, axisymmetric waves were the first formed by the motion of our kink-wave generator. Figure 7 shows a typical example of an axisymmetric wave propagating ahead of, and away from, a kink wave. Axisymmetric waves become unstable at relatively small amplitudes and cause vortex breakdown as the perturbations grow. Because most uncontrolled perturbations imposed on a vortex will generate axisymmetric waves in addition to torsional waves, we believe that these waves were present also in the turbulent system of HBG, and in fact this form of vortex breakdown was responsible for most of the observed small-scale turbulent events. The axisymmetric waves were probably overlooked by HBG because of the small amplitude required for instability to occur.

Vortex breakdown has many technical applications (e.g. Lambourne & Byer 1961) and has therefore been extensively studied as a stationary wave phenomenon related to a change in flow conditions. The most complete theoretical description we know of is due to Benjamin (1962, 1967(*a*)) which has considerable experimental support in the work of Escudier, Bornstein & Zehnder (1980), Escudier, Bornstein & Maxworthy (1982), among others. Essentially, the view is that a weak vortex breakdown consists of a standing train of finite-amplitude waves each of which closely approximates a 'sech^2' solitary wave solution. When the leading wave reaches a certain critical amplitude, the wake-like flow field created in its interior becomes unstable to spiral disturbances of negative wavenumber (see figure 12), a point of view espoused by Escudier *et al.* (1982) based on the work of Lessen, Singh & Paillet (1972). In any experiment, these invariably grow to become unstable, finite-amplitude spirals of small pitch rotating in a direction opposite to that of the basic rotation. In the sense of the wave experiments of §4, the wave pattern achieves a pitch that allows it to move at a velocity equal to the wave speed of the axisymmetric solitary wave. Often this disturbance grows so rapidly that it completely dominates the flow visualization of the phenomena, so that usually any sense of an axisymmetric wave is lost, although it still exists in the mean flow, of course, and is central to a complete understanding of the whole phenomenon.

Clearly, by a simple Galilean transformation, these standing waves on a supercritical axial velocity can be replaced by considering travelling waves on a subcritical flow as studied theoretically and experimentally by Pritchard (1970) and demonstrated earlier in the experiments of Granger (1968). In the latter, the axial outlet of a vortex flow similar to ours was suddenly completely closed and this information transmitted to the core via an unstable, axisymmetric, travelling vortex breakdown. By judicious adjustment of this closing process, we have found that it is possible to form the whole range of vortex breakdown types from a weak solitary wave to a violent breakdown of the type described by Granger (1968). As already mentioned above, anything one does to a vortex core results in the formation of at least one weak solitary wave. Here we are reminded of the exactly analogous situation in a stratified fluid (Benjamin 1967(*b*), Davis & Acrivos 1967, Maxworthy 1980) where the first wave to leave a region of disturbed fluid was a symmetric internal gravity wave exactly analogous to the axisymmetric type on a vortex core (Pritchard 1970).

A complete study of the stability of axisymmetric travelling waves is beyond the objectives of this paper. Recent calculations carried out in Maxworthy *et al.* (1983), based on Benjamin's (1967*a*) formulation, showed, however, that an axisymmetric wave with about a 20 % increase in vortex core radius gives rise already to an unstable

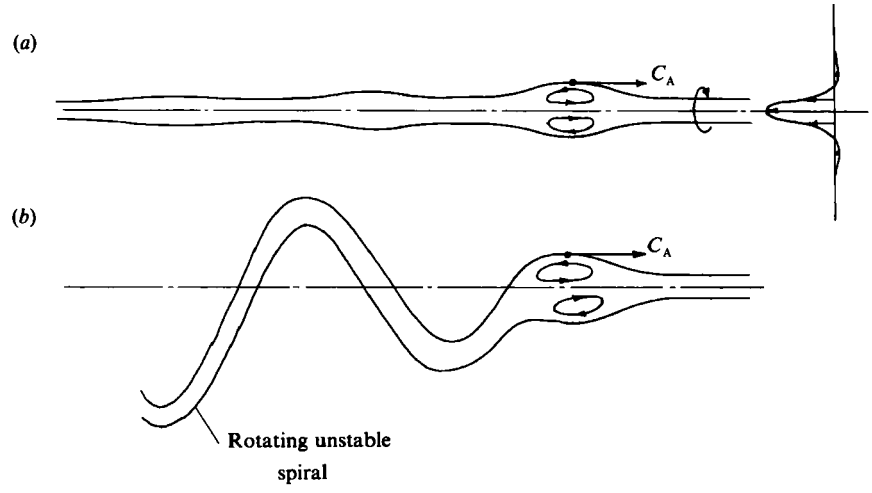

FIGURE 12. Sketch of axisymmetric vortex waves: (*a*) train of axisymmetric waves on a vortex core ordered by amplitude; (*b*) large-amplitude solitary wave which causes the flow behind it to become unstable to spiral disturbances, evolving often to turbulence.

situation qualitatively in agreement with our observations. The calculations show furthermore that the effect of the axial velocity profile on the wave speed is

$$C = V_m \pm 0.93 W_m$$

where the plus or minus sign depends on whether the wave travels with or against the axial flow in the vortex core.

8. Discussion

8.1. *Waves on 'controlled' vortex flows*

We have observed at least six different types of waves on a well-controlled vortex flow. Two of these, the helix and the standing wave, are regular in the sense that they have a well-defined wavelength and amplitude which do not vary appreciably along the length of the tank. These and the other types of kink wave, the isolated kink, the isolated kink plus trailing disturbance and the disturbance with increasing wavelength, have been observed to be extremely stable entities which do not cause disruption of the vortex core. Even when they interact quite violently, the core remains unbroken. When a kink wave is formed by disrupting the core, the latter reforms through the propagation of a wave of contraction from the suction tube, which reconcentrates the disrupted vortex lines. As the waves propagate they appear to have no effect upon the core flow – there is no dramatic thinning or vortex concentration, which would suggest that the kink waves could be important in the formation of the cores themselves.

On the other hand, the axisymmetric waves, even at relatively small amplitude, do disrupt the core, creating tightly wound helices and turbulence; here again the cores are reformed by the propagation of a wave of contraction from the suction tube which reorganizes the vortex lines. These results are important in the interpretation of the wave motions observed in less-controlled circumstances, as we discuss in §8.2.

	Upward-propagating, axisymmetric and unstable	Downward-propagating, axisymmetric and unstable	Upward-propagating, kinks	Downward-propagating, kinks
Sequence 1 (3 cores, 25 s duration)	10	3	1	0
Sequence 2 (2 cores, 36 s)	17	3	4	1
Sequence 3 (3 cores, 55 s)	21	7	4	0
Totals	48	13	9	1
Percentage	67	18.5	13	1.5

TABLE 1. Frequency of occurrence of unstable axisymmetric waves in the turbulent system studied by HBG

8.2. *Waves in turbulent rotating fluids*

Here we reexamine the results of HBG, noting, among other things, the preponderance of unstable axisymmetric waves, and add some extra observations to emphasize this point.

The critical observation here is that any disturbance that tends to cut off or reduce the axial flow in the vortex core creates an axisymmetric type of solitary wave, which may or may not become unstable, depending on its amplitude. In the experiments of HBG the axial flow in the cores was downward into the mixed region (see figure 13); at frequent intervals this axial flow was cut off completely by the turbulent motion in the mixed layer, and this information was transmitted along the core to the rest of the fluid by a wave of such large amplitude that it was invariably unstable. In the light of what we know now about unstable axisymmetric travelling waves, and vortex breakdown such a wave can be clearly seen in HBG (figures 16*c* and 12). If such a flow reduction is caused by disturbances above the mixed layer as by the very intense interaction of kink waves, then this too will produce unstable 'axisymmetric waves' as in figures 16(*a*, *b*) of HBG. Owing to the asymmetry of this process, the most-unstable waves propagate against the axial flow, i.e. upwards, while the downward-propagating ones, which are usually not seem in the visualization, cause little disruption. The axial flow into the mixed layer is maintained, and this causes a wave of contraction upwards into the disturbed region, which reestablishes the axial flow.

From the photographs in HBG, reexamination of their films and our own observations, reported here, it is clear that upward-propagating unstable axisymmetric waves are of critical importance in the dynamics of the flow above the mixed layer. We note especially that they create regions of small-scale turbulence well above the mixed region, and hence must be responsible for a large part of the dissipation that occurs there.

Finally, we have attempted to quantify these observations by noting over a certain time the number of each type of wave that crosses a given central cross-section of the tube for several sequences, consisting of different forcing frequencies and hence number of cores (table 1).

Although the designations are somewhat subjective, by now we have had enough experience to be able to determine the wave types correctly in at least 8 out of 10 cases. We note the clear preference for unstable, upward-propagating waves and the

relative paucity of well-defined kink waves of small wavelength and long lifetime. Of course, the general wandering of the vortex cores and waves of a length comparable to the length of the tank might also be interpreted as kink waves, but we have not included them in the above classification since they do not contribute substantially to the dissipative processes in the quasi-two-dimensional turbulence regime well above the grid and are very difficult to observe unequivocally.

This work was supported at the University of Grenoble by CNEXO contract 83/2846 and USC by ONR contract N00014-82-K-0084.

We greatly appreciate the help of Serge Layat and many crucial discussions with F. K. Browand, P. Huerre and in particular M. Mory. The first version of this paper was reviewed by Professor D. W. Moore of Imperial College, who, among other things, brought the critically important paper by Moore & Saffman (1972) to our attention. The use of results from that paper greatly expanded the scope and possible importance of our work, and we are deeply indebted to Professor Moore for his perceptive review and subsequent interest in our efforts.

Appendix. The formation of concentrated vortices in rotating, turbulent flow

The formation of concentrated vortices requires two major ingredients, a relatively weak ambient or background vorticity and some meridional flow that then convects the vorticity towards a suitable central location (Maxworthy 1981). Thereafter, the vorticity convection mechanism and diffusion by viscosity compete to produce a steady-state configuration. In some cases it has been observed that axisymmetric, inertial wave propagation is able to bring about the penetration of a localized convection mechanism into the main body of the rotating fluid (Gluck 1972), and vortex concentration or spin-up occurs rapidly. HGB's observations of rapid vortex formation suggest that some similar mechanism is at work which we motivate as follows. In the present case, upon starting the grid oscillation, a front separating turbulent from nonturbulent fluid was created. Behind the front the turbulence was three-dimensional and describable by the non-rotating experiments of Hopfinger & Toly (1976) for example. This front propagated until a critical value of the local Rossby number based upon the magnitude of the local turbulent velocity fluctuations and integral scale was reached. Thereafter vortex generation occurred in a time corresponding to the travel time of inertial waves along the fluid column. In some less-extensive observations of the transient state, Dickinson & Long (1983) noted that when the critical value of the local Rossby number was reached the front broke down into a number of fluid columns, which penetrated upwards in the form of cones constituting the envelope of upward-propagating inertial waves, in a manner entirely equivalent to the formation of a Taylor column, in front of a body being moved along the axis of a rotating fluid (Maxworthy 1970). The upward dye-propagation velocity v was measured by these authors to be proportional to $(K\Omega)^{\frac{1}{2}}$, where $K = u_T l_T$ (here u_T and l_T are the magnitudes of the velocity fluctuations and integral scales at the plane of column formation, respectively).

Dickinson & Long's observations are analogous to observations of turbulent front propagation and generation of two-dimensional slug flows by grid oscillation in a stratified flow. Here in an entirely equivalent manner when a critical Richardson number was reached at the front it collapsed into a number of wedge-shaped regions or fingers, which penetrated the ambient fluid, generating internal waves as they did

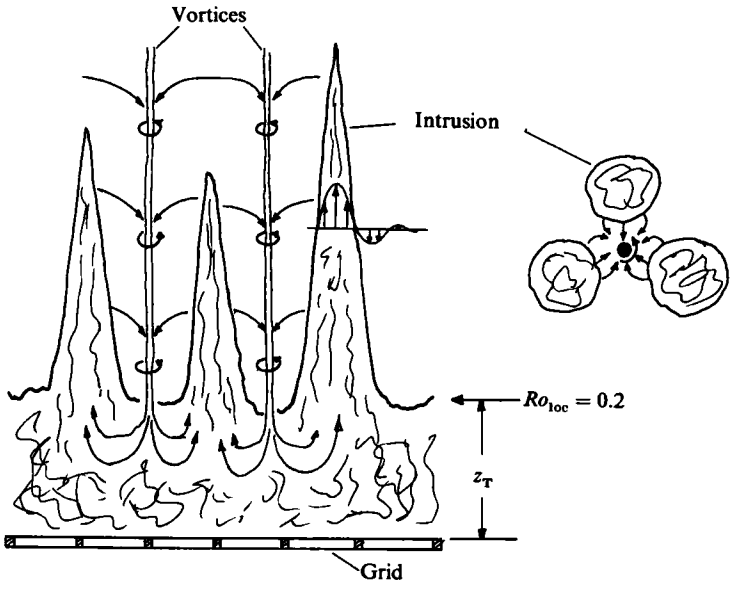

FIGURE 13. Formation of concentrated vortices by turbulence in a rotating fluid. The rising columns of mixed fluid, created by turbulence, collapse at a critical local Rossby number, causing a convergence of fluid, which concentrates vorticity and forms an intense vortex.

so (Ivey & Corcos 1982; Browand & Hopfinger 1981, 1983; Thorpe 1982). A study of the geometry and flow fields in both cases reveals that a convergent flow field must be produced between the cones or wedges by the divergent flow they create. In particular, for the rotating-flow case, the most-intense effect will be felt at the centre of the triangle formed by three rising fluid columns. This process is shown diagrammatically in figure 13, where it can be seen that the tendency to vortex concentration should be greatest between the rising columns, but more critically that the amount of vortex concentration can far outweigh the amount of vortex compression and anticyclonic vortex formation caused by the rising columns. Thus eventually the cyclonic vortices dominate the flow, while the anticyclonic vorticity which is distributed throughout the fluid has a dominating effect only at the outer wall of the container, where cyclones are less likely to form. Clearly a similar intensification of the density gradient between the intrusions also occurs in the stratified-flow case, but its effect is not so dramatic in such a two-dimensional flow.

REFERENCES

ARMS, R. J. & HAMA, F. R. 1965 Localized-induction concept on a curved vortex and motion of an elliptic vortex ring. *Phys. Fluids* **8**, 553–559.

BATCHELOR, G. B. 1967 *An Introduction to Fluid Dynamics*. Cambridge University Press.

BENJAMIN, T. B. 1962 Theory of the vortex breakdown phenomenon. *J. Fluid Mech.* **14**, 593–629.

BENJAMIN, T. B. 1967*a* Some developments in the theory of vortex breakdown. *J. Fluid Mech.* **28**, 65–84.

BENJAMIN, T. B. 1967*b* Internal waves of permanent form in fluids of great depth. *J. Fluid Mech.* **29**, 559–592.

BETCHOV, R. 1965 On the curvature and torsion of an isolated vortex filament. *J. Fluid Mech.* **22**, 471–479.

BROWAND, F. K. & HOPFINGER, E. J. 1981 Spread of turbulence into stratified fluid. *APS Meeting, paper* D.E. 1.

BROWAND, F. K. & HOPFINGER, E. J. 1983 The inhibition of vertical turbulent scale by stable stratification. In *IMA Conf. Proc., Cambridge.*

BURGERS, J. M. 1948 A mathematical model illustrating the theory of turbulence. *Adv. Appl. Mech.* **1**, 171–199.

CROW, S. H. 1970 Stability theory for a pair of trailing vortices. *AIAA J.* **8**, 1731.

DAVIS, R. E. & ACRIVOS, A. 1967 Solitary internal waves in deep water. *J. Fluid Mech.* **29**, 593–607.

DICKINSON, S. C. & LONG, R. R. 1983 Oscillating grid turbulence including effects of rotation. *J. Fluid Mech.* **126**, 315–333.

ESCUDIER, M. P., BORNSTEIN, J. & MAXWORTHY, T. 1982 The dynamics of confined vortices. *Proc. R. Soc. Lond.* A **382**, 335–360.

ESCUDIER, M. P., BORNSTEIN, J. & ZEHNDER, N. 1980 Observations and LDA measurements of confined vortex flow. *J. Fluid Mech.* **98**, 49–63.

GARG, A. K. & LEIBOVICH, S. 1979 Spectral characteristics of vortex breakdown flow fields. *Phys. Fluids* **22**, 2053–2070.

GLUCK, D. F. 1972 Vortex formation, free surface deformation and flow field structure in the discharge of liquid from a rotating tank. Ph.D. dissertation, University of Southern California, Los Angeles; also *North American Rockwell Corp. Rep.* 5072-SA-0108.

GRANGER, R. 1968 Speed of a surge in a bathtub vortex. *J. Fluid Mech.* **34**, 651–656.

HARVEY, J. K. 1962 Some observations of the vortex breakdown phenomenon. *J. Fluid Mech.* **14**, 585–592.

HASIMOTO, H. 1972 A soliton on a vortex filament. *J. Fluid Mech.* **51**, 477–485.

HOPFINGER, E. J. & BROWAND, F. K. 1982 Vortex solitary waves in a rotating, turbulent flow. *Nature* **295**, 393–396.

HOPFINGER, E. J., BROWAND, F. K. & GAGNE, Y. 1982 Turbulence and waves in a rotating tank. *J. Fluid Mech.* **125**, 505–534.

HOPFINGER, E. J. & TOLY, J. A. 1976 Spatially decaying turbulence and its relation to mixing across density interfaces. *J. Fluid Mech.* **78**, 155–176.

IVEY, G. N. & CORCOS, G. M. 1982 Boundary mixing in a stratified fluid. *J. Fluid Mech.* **121**, 1–26.

KIDA, S. 1981 A vortex filament moving without change of form. *J. Fluid Mech.* **112**, 397–409.

LAMB, G. L. 1980 *Elements of Soliton Theory.* Wiley-Interscience.

LAMBOURNE, N. C. & BYER, D. W. 1961 The bursting of leading edge vortices – some observations and discussion of the phenomenon. *Aero. Res. Counc. R & M* 3282.

LEIBOVICH, S. 1970 Weakly non-linear waves in rotating fluids. *J. Fluid Mech.* **42**, 803–822.

LEIBOVICH, S. & MA, H. Y. 1983 Soliton propagation on vortex cores and the Hasimoto soliton. *Phys. Fluids* **26**, 3173–3179.

LESSEN, M., SINGH, P. J. & PAILLET, F. 1974 The stability of a trailing line vortex. Part 1. Inviscid theory. *J. Fluid Mech.* **63**, 753–763.

LEVY, H. & FORSDYKE, A. G. 1928 The steady motion and stability of a helical vortex. *Proc. R. Soc. Lond.* A **120**, 670–690.

MAXWORTHY, T. 1970 The flow created by a sphere moving along the axis of a rotating, slightly viscous fluid. *J. Fluid Mech.* **40**, 453–479.

MAXWORTHY, T. 1972 On the structure of concentrated, columnar vortices. *Astro. Acta* **17**, 363–374.

MAXWORTHY, T. 1980 On the formation of nonlinear internal waves from the gravitational collapse of mixed regions in two and three dimensions. *J. Fluid Mech.* **96**, 47–64.

MAXWORTHY, T. 1981 The laboratory modelling of atmospheric vortices: a critical review. In *Intense Atmospheric Vortices* (ed. L. Bengtsson & J. Lighthill), pp. 229–246. Springer.

MAXWORTHY, T., MORY, M. & HOPFINGER, E. J. 1983 Waves on vortex cores and their relation to vortex breakdown. In *Proc. AGARD Conf. on Aerodynamics of Vertical Type Flows in Three Dimensions; AGARD* CPP-342, *paper* 29.

MOORE, D. N. & SAFFMAN, P. G. 1972 The notion of a vortex filament with axial flow. *Phil. Trans. R. Soc. Lond.* A **272**, 403–429.

POCKLINGTON, H. C. 1895 The complete system of the periods of a hollow vortex ring. *Phil. Trans. R. Soc. Lond.* A **186**, 603.

PRITCHARD, W. G. 1970 Solitary waves in rotating fluids. *J. Fluid Mech.* **42**, 61–83.

SALLET, R. S. & WIDMEYER, D. W. 1974 An experimental investigation of laminar and turbulent vortex rings in air. *Z. Flugwiss.* **22**, 207–215.

SARPKAYA, T. 1971 On stationary and travelling vortex breakdown. *J. Fluid Mech.* **45**, 545–559.

SQUIRE, H. B. 1962 Analysis of the vortex breakdown phenomenon. Part I. *Miszellanen der angew. Mech.* 306–312, *Akademie Berlin.*

THOMSON, W. 1880 On the vibrations of a columnar vortex. *Phil. Mag.* (5) **10**, 155.

THORPE, S. A. 1982 On the layers produced by rapidly oscillating a vertical grid in a uniformly stratified fluid. *J. Fluid Mech.* **124**, 391–409.

YUEN, H. C. & LAKE, B. M. 1975 Non linear deep water waves: theory and experiment. *Phys. Fluids* **18**, 956–960.